QUARTERLY JOURNAL
OF THE
ROYAL METEOROLOGICAL SOCIETY

Vol. 108 OCTOBER 1982 No. 458

Quart. J. R. Met. Soc. (1982), **108**, pp. 739–762

551.515.41:551.558.1:551.576.11

Two-dimensional convection in non-constant shear: a model of mid-latitude squall lines

By A. J. THORPE*, M. J. MILLER and M. W. MONCRIEFF

Atmospheric Physics Group, Imperial College, London

(Received 8 July 1981; revised 2 February 1982)

SUMMARY

Numerical simulations of two-dimensional deep convection are analysed using analytical models extended to include shallow downdraughts and non-constant shear. The cumulonimbus are initiated by low-level convergence created by a finite amplitude downdraught. These experiments have constant low-level shear and differ only in the profile of mid- and upper-level winds. Quasi-steady convection is produced if the mid- and upper-level flow has small shear and the low-level shear is large. The surface precipitation is maximized for no initial relative flow aloft and, if stationary, this storm ($P(O)$) can give prodigious localized rainfall; $P(O)$ is the two-dimensional equivalent of the supercell. These results are placed in context with previous two-dimensional simulations. Attention is drawn to the similarity with squall lines in central and eastern U.S.A.

Storm $P(O)$ is analysed by construction of time-averaged fields of streamfunction, vorticity, temperature, and height deviation. The smoothness of these fields suggests a conceptual model of the storm dynamics which involves cooperation between distinct characteristic flows; an overturning updraught, a jump type updraught, a shallow downdraught, a low-level rotor, and a boundary layer.

An idealized analytical model is described by solution of the equations for steady convection. These solutions, for the remote flow, are derived from energy conservation, mass continuity and a momentum budget, and they give relationships between the non-dimensional parameters of the problem. It is apparent that the convection is a high Froude (or low Richardson) number flow demanding the existence of a cross-storm pressure gradient. Inherent in this idealized model is a vortex sheet between updraught and downdraught and it is considered that the dynamical instability of this sheet is related to complexities in the numerical simulation. Furthermore, these results show that in two-dimensions both non-constant shear and a shallow downdraught are necessary to maintain steady convection.

1. INTRODUCTION

The earliest attempts at modelling cumulonimbus exploited the practical advantages of two-dimensional flow. Several such models emerged and the first investigations into the effects of ambient wind shear were described (Orville 1968; Takeda 1971; Schlesinger 1973; Hane 1973 and Wilhelmson 1974). Rather rapidly most of these models were abandoned in favour of three-dimensional ones, and the most recent examples are described in Miller (1978), Klemp and Wilhelmson (1978), Clark (1979), and Schlesinger (1980). The three-dimensional models represent substantial improvements, not only due to their physical realism but also due to better understanding of the numerical solutions of the equations of motion. This paper returns to the two-dimensional case to re-examine the problem of 'steady' cumulonimbus, particularly as both modelling expertise and the understanding of convective dynamics have advanced considerably since the early studies. It is also one of a series of papers by the authors which attempts to quantify the role of the downdraught in the initiation, regeneration, and maintenance of cumulonimbus. Furthermore, it is timely to re-examine two-dimensional models in the light of the work of Moncrieff (1978), which proved the impossibility of steady overturning in constant shear with a deep downdraught.

In Thorpe, Miller and Moncrieff (1980; hereafter referred to as TMM), the response of

*Present address: Department of Meteorology, University of Reading.

an unsheared atmosphere to the presence of a constant low-level heat sink was considered. This description of the dynamics of downdraughts assumed a dry atmosphere so that although low-level convergence was produced, moist convection could not take place. In this paper simulations with moisture are described. A heat sink present initially is switched off after 15 min, allowing evaporation from rain to maintain the downdraught. The initial cooling creates cold air which spreads upstream at low-levels, thus producing convergence and allowing moist convective cells to grow. Evaporation from rain may then occur at the same location as the initial heat sink. This process is influenced mainly by the ambient wind profile. The results of a set of numerical experiments which differ only in the assumed mid- and upper-level winds, are presented here.

It is interesting to relate these simulations to earlier two-dimensional results. One important difference is that they used different initiation techniques and this will be discussed later. All the models use similar wet unstable thermodynamic soundings, the crucial physical difference being in the profile of the ambient wind. The profiles can be grouped into three types:

Type A – constant shear – S, W, T (B3, B5), H (R1, R2, R3, R5), O
Type B – reverse shear – T (C7, C8, C9, C10)
Type C – low level shear – H (R4)

(where S-Schlesinger, W-Wilhelmson, T-Takeda, O-Orville, H-Hane).

In A, the shears are nearly constant but the values differ. In summary, they produce a cumulonimbus lasting up to one hour and moving with a mid-tropospheric (on average) wind speed. It eventually dissipates due to the downshear sloping updraught releasing rain into the buoyant inflow air, thus disrupting the storm's inflow. Such simulations appear to be well represented by the dynamical solutions of Moncrieff and Green (1972) and Moncrieff (1978), except that the simulations had shallower downdraughts. This comparison will be taken further in Section 5(d).

In B, used by Takeda (1971) there is a jet at various levels with approximately constant shear above and below the jet level. Although these simulations can be criticized for certain numerical problems and a vagueness in quoting the storm's speed, they draw attention to the importance of the upshear low-level slope of the updraught produced by the negative shear there. The profile producing the longest-lived storm was C8, which bears a similarity to that associated with tropical squall-lines. The relationship of this simulation to that of Moncrieff and Miller (1976) is of interest as they imply that the steady squall-line convection must be three-dimensional.

Finally C, which has low-level shear and constant mid- and upper-level winds, has only been considered by Hane (1973) in the simulation R4. Unfortunately, R4 is not discussed in detail in that paper except to say that it produced a long-lasting storm which moved with the constant wind speed of the mid- and upper-levels. The following discussion considers several profiles, one of which is very similar to R4.

2. Numerical simulations

(a) *Initial conditions*

Cumulonimbus simulations are usually initiated either by an elevated warm bubble or by orographic forcing. In the former method the first cell may be polluted with structure produced merely from the details of the bubble (Clark 1979), which can at best only be a crude approximation to natural initiation mechanisms. Orographic forcing has, perhaps, a more precise physical basis, but suffers from being relevant to only particular geographical locations.

The simulations to be described here are initiated by specifying an initial localized cooling region which attempts to model evaporative cooling from an initial cell. The only dynamical detail of this cell modelled is that its evaporation is stationary in the low-level

flow. This technique avoids certain of the difficulties of the other methods but obviously has its own limitations.

The basic model details are as described in TMM, except that moisture is included by using the q and θ profile from Miller (1978), which describes the simulation of the Hampstead storm. The model domain is 50 km by 900 mb with $\Delta x = 500$ m and $\Delta p = 50$ mb. The heat sink $Q(p, t)$ is as follows:

$$\begin{aligned} t \leqslant 15\,\text{min} \quad & Q = Q_c && 1000 > p > 850\,\text{mb} \\ & = Q_c(p - 750)/100 && 850 > p > 750\,\text{mb} \\ & = 0 && 750 > p \\ 15 < t < 21\,\text{min} \quad & Q = (21 - t)Q(t = 15)/6 \\ t > 21\,\text{min} \quad & Q = 0 \end{aligned}$$

where Q_c is a constant cooling rate, based on evaporation rates calculated from previous simulations.

The results will be described in a reference frame fixed with the heat sink and so the ambient flow is relative to this sink. The problem of the development of the sink, or rainfall, will not be discussed in this paper, and so the arguments presented analyse the maintenance but not the development of a steady state.

Initially, a constant ambient wind, u_0, was chosen so as to maintain continuity with the results of TMM, which showed that the upstream gust front is not stationary unless $|u_0| \gtrsim 15\,\text{m s}^{-1}$. Such a quasi-stationary gust front producing localized boundary layer convergence is clearly essential in the production of a long-lived storm. Thus the first simulation had constant $|u_0| = 15\,\text{m s}^{-1}$ and $Q_c = -0{\cdot}5\,^{\circ}\text{C min}^{-1}$. No substantial convective cells were produced in this simulation for the following reasons. As noted in TMM, above the upstream density current there is a significant inflow produced by the pressure field of the sink. This inflow along with the ambient flow of $15\,\text{m s}^{-1}$ meant that there was a very large shear between the surface (where at the upstream gust front $u \simeq 0$) and 700 mb, which acts to dissipate the convection. It now becomes clear that to reduce this effective shear it is necessary to have smaller ambient inflow near cloud base.

In Fig. 1 the five profiles of u to be considered in this paper are plotted. All five have constant shear below 2·5 km – the value of the average wind (0–2·5 km) being chosen so as to most nearly keep the upstream gust front stationary. It was decided to use $Q_c = -0{\cdot}6\,^{\circ}\text{C}$

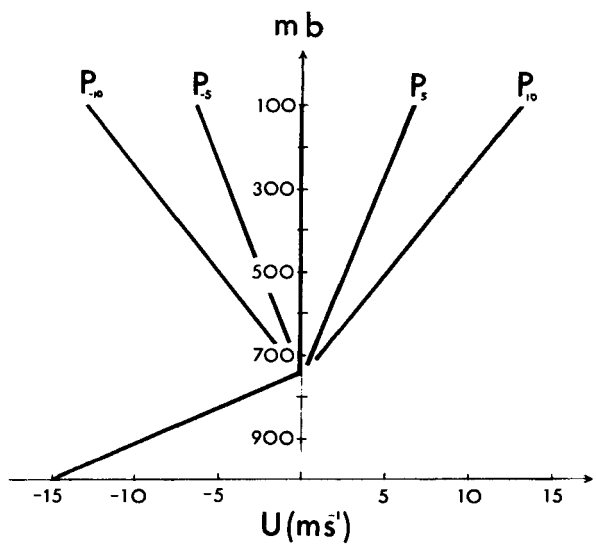

Figure 1. Profiles of the initial flow used in the simulations.

min^{-1} and $u_s = u(z = 0) = -15\,\text{m s}^{-1}$. The profiles above $z = 2{\cdot}5\,\text{km}$ attempt to explore physically interesting situations; $P(+10)$ and $P(-10)$ model a mid-latitude shear and a (tropical) jet profile respectively. The three profiles $P(-5)$, $P(0)$, and $P(+5)$ complete the examination of this region of parameter space (note that $P(0)$ is similar to $H(R4)$).

In summary, it has been argued that for this type of downdraught-maintained convection, it is immediately apparent that low-level shear is a desirable and necessary feature. The results of TMM have helped to set values of u_s and Q_c which can produce a stationary upstream gust front and the possibility of steady convection. The simulations will now explore the influence of the wind profile above 2·5 km on the subsequent convection. (It should be noted that although the initial downdraught forcing is assumed stationary, the cloud can propagate when the forcing is removed. The influence of this initial assumption will be discussed later.)

The value of the raindrop evaporation constant was chosen to be $\beta = 0{\cdot}0005\,\text{s}^{-1}$ to ensure that the cooling produced by the heat sink was approximately matched to that produced by evaporation from raindrops. There is clearly an optimum set of values of $\{Q_c, u_s, \text{CAPE}, q, \text{and } \beta\}$ (where CAPE is the convective available potential energy and q is the specific humidity) to keep the upstream gust front stationary, i.e. changing one parameter requires a compensatory change in the others. This optimization is a subject of current research and is probably indicative of the somewhat special conditions needed for the occurrence in nature of the storms to be described. However, in this paper the values chosen are kept constant.

(*b*) *Rainfall characteristics and storm motion*

A complete description of the characteristics of these five simulations is beyond the scope of this paper; the next section will concentrate on $P(0)$. However, some general comparisons between the storms can be made involving the rainfall, steadiness, and propagation characteristics. Each of the simulated storms has essentially the same available moisture flux to process and produce rain at the surface, because the inflow below 2·5 km is approximately the same in each case. Therefore the precipitation efficiency of the storm is given by the rainfall totals. In Fig. 2 the rainfall distribution at $t = 96\,\text{min}$ is plotted for each storm with the position of the maximum increment since $t = 90\,\text{min}$ and the total rainfall (i.e. areal sum) also shown. The total rainfall values show that $P(0)$ is the most efficient storm, producing about 30% more rain than $P(+5)$ by 96 min. The profiles with the upper winds in opposition to the lower wind give storms which are more efficient in producing rainfall than their counterparts.

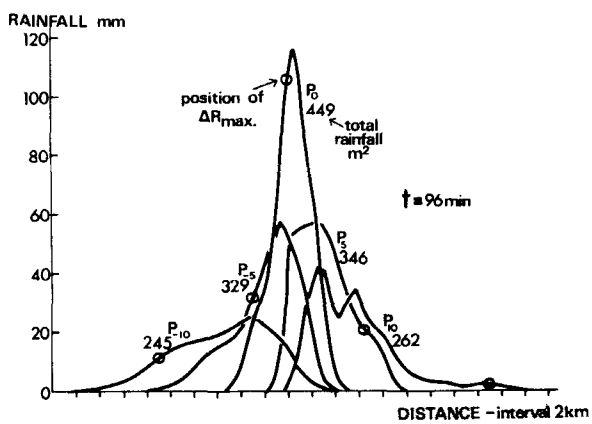

Figure 2. Rainfall distribution at $t = 96\,\text{min}$ for the five simulations. The position of the maximum increment in rainfall since 90 min and the total rainfall (i.e. $\int R\,dx$) are also indicated.

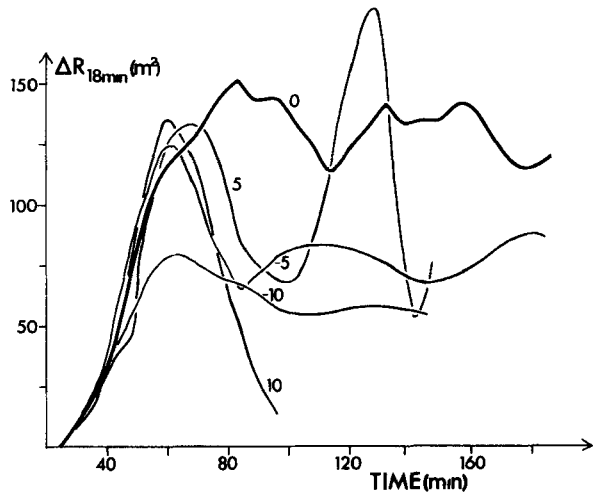

Figure 3. Total rainfall increment in the previous 18 min as a function of time.

The width of the rainfall distribution in Fig. 2 is dependent on the storm motion and the slope of the updraught. Although it is tempting to attribute this feature to the motion alone, detailed analysis of these simulations shows that updraught slope is a more important factor. The tendency for motion is indicated by the position of the maximum increment in rainfall in the period 90–96 min, shown on Fig. 2. However, this motion away from the site of the initial forcing is not, in general, consistently maintained. It is clear, however, that $P(0)$ is a localized and, in this reference frame, stationary storm.

To explore this problem further, the rainfall increment in the previous 18 min was evaluated as a function of time (see Fig. 3). Storm $P(0)$ is quasi-steady and the most intense; while $P(+5)$ and $P(+10)$ are clearly unsteady, with $P(+10)$ decaying completely. Interestingly, storm $P(+5)$ produces a vigorous second cell which, however, also decays rapidly. The storms $P(-5)$ and $P(-10)$ are less vigorous but nevertheless, quasi-steady. This has interesting parallels with the results of Moncrieff (1978) and Moncrieff and Miller (1976). The dynamical structure indicates, however, that these jet profile storms are multicellular. In particular, $P(-10)$ is composed of discrete cells which were generated at the upstream gust front and moved at about $-3\,\mathrm{m\,s^{-1}}$ before decaying after about 30 min. The cellular structure, which is distinct from the single cell ($P(0)$), is apparent in Fig. 8(b) to be described later. A consequence of this cellular structure is that there was increased evaporation from rainfall causing the upstream gust front to move upstream, allowing the storm to propagate relative to the winds at all levels. Such propagation is typical of tropical storms with a jet-like wind profile. These ideas are the subject of further research.

In summary, the storm $P(0)$ is localized and stationary in the model reference frame. Furthermore, it produces the maximum total rainfall of the five simulated storms. All cases required strong low-level shear to prevent the upstream gust-front from propagating rapidly away from the storm.

3. Structure of storm $P(0)$

The rainfall characteristics of $P(0)$ indicate an underlying quasi-steady structure to the convection. To investigate this instantaneous and time-averaged fields will be considered. It is expected that the time-averages will only be meaningful if the storm has a basic steady character, the extra details of the time-dependent fields being a superimposed 'turbulence'.

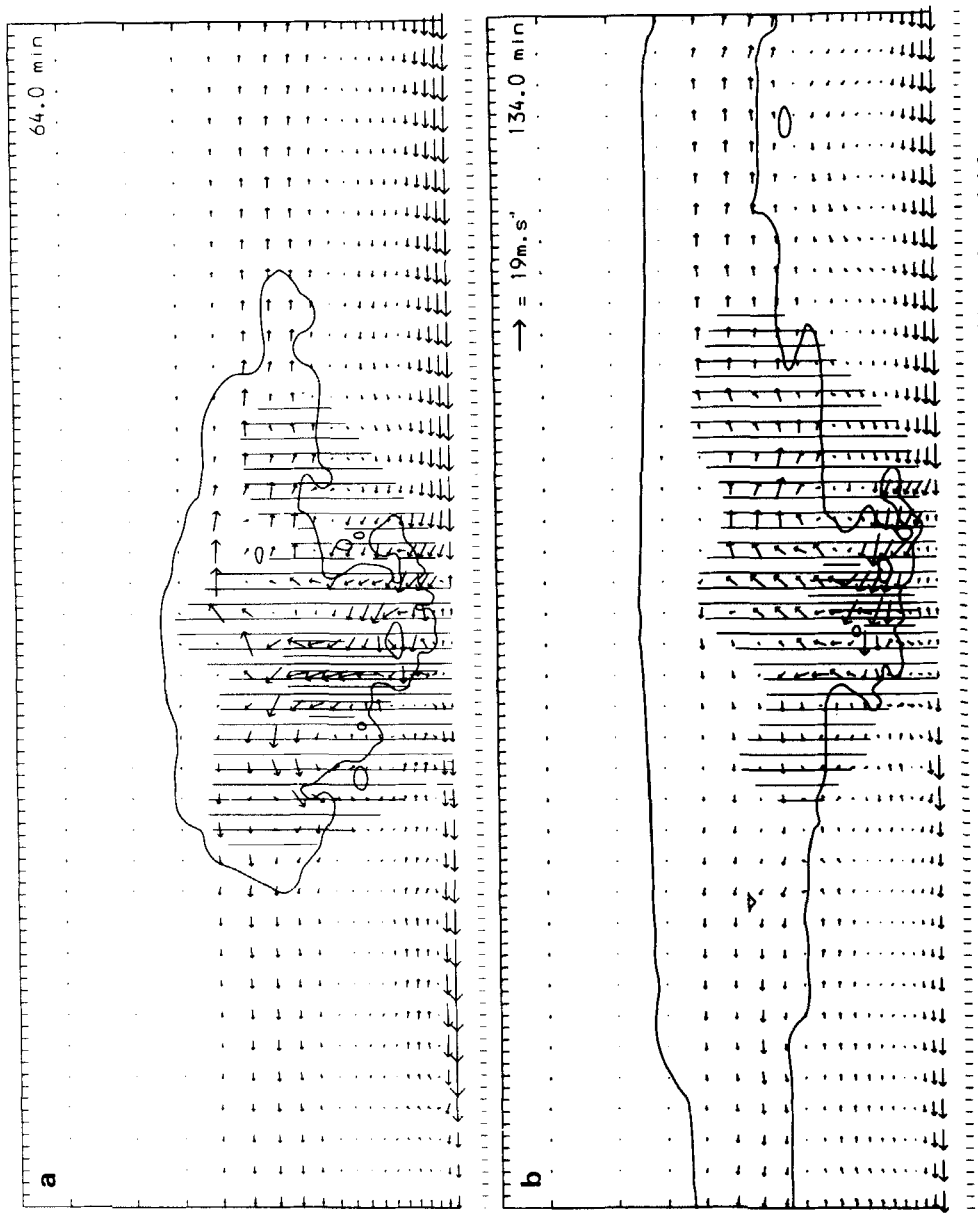

Figure 4. (a) Cross section of cloud, rain and velocity vectors at $t = 64$ min for $P(0)$. Horizontal ticks every 500 m and vertical ticks every 50 mb. Except for Fig. 8 all simulation results refer to $P(0)$. (b) As in (a) at $t = 134$ min.

(*a*) *Evolution and trajectories*

In Figs. 4(a), 4(b), the structure of the storm $P(0)$ is shown in vertical cross-sections on which are plotted cloud outline, light and heavy rain and velocity arrows. They refer to $t = 64$ min and $t = 134$ min respectively. The low-level inflow from the right is clearly shown and this air is peeled away from the surface layers into an arch cloud before entering the main cloud updraught. The heavy rain falling from the updraught maintains a downdraught circulation whose source of air is from the left of the storm in the layer $850 > p > 750$ mb. This air descends under the main updraught and flows both to the right and left when spreading out at the surface. To the right (upstream) a gust front is formed between downdraught air and the ambient inflow. The downstream near-surface outflow propagates freely away from the storm and out of the left boundary. (The improved lateral boundary

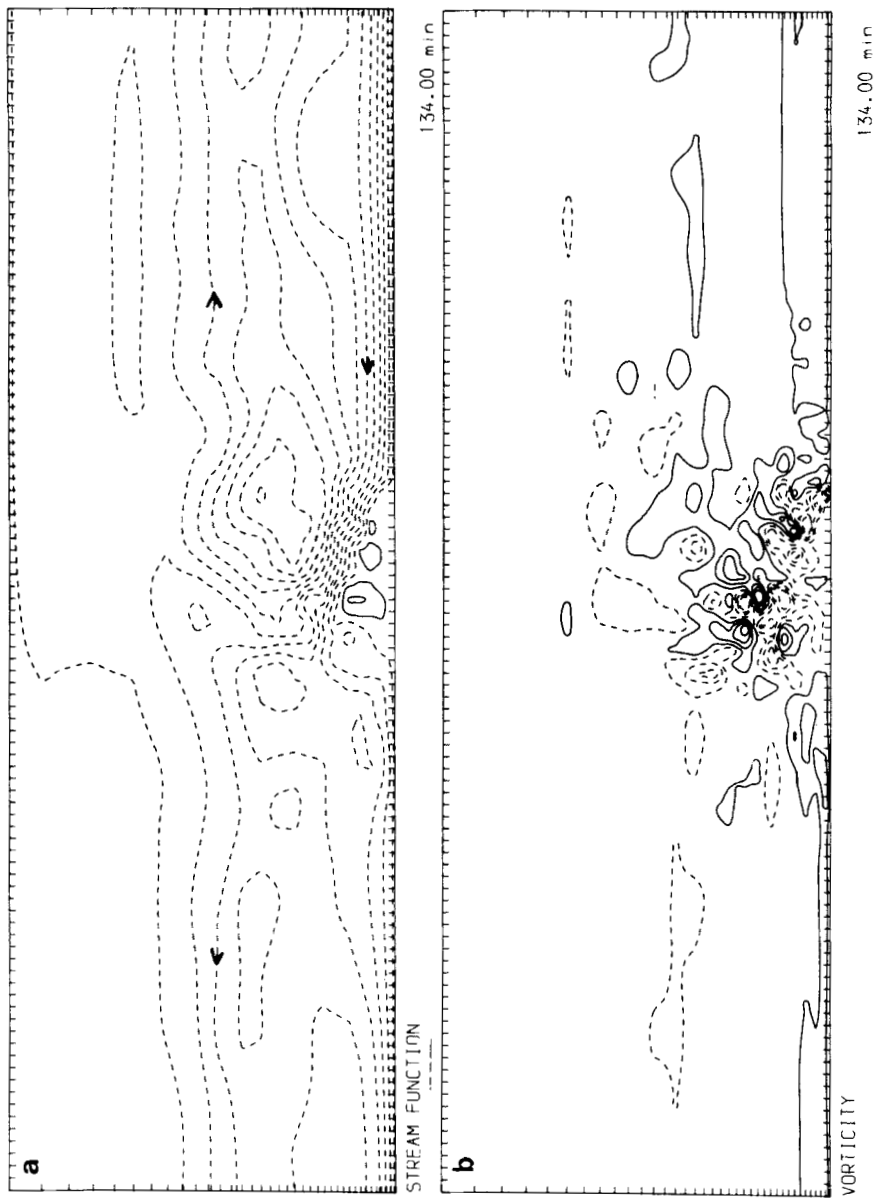

Figure 5. (a) As in Fig. 4 (b) for streamfunction ($\Delta\psi = 3000\,m^2s^{-1}$). (b) As in (a) for vorticity ($\Delta\eta = 0{\cdot}005\,s^{-1}$).

conditions used in TMM and in this paper are described in Miller and Thorpe, 1981.) To the left of the storm, the low-level flow no longer retains 'memory' of the ambient flow at these levels.

Cross-sections of streamfunction, vorticity, potential temperature and height deviation are shown in Figs. 5(a) and (b), 6(a) and (b)at $t = 134$ min. The vorticity field has a lot of fine structure in the updraught region, due to individual thermals, but several predominant features are evident. The positive vorticity maximum on outflow is produced by generation of vorticity along trajectories arising from the horizontal gradient of potential temperature. There is a narrow zone of negative vorticity between the updraught and the upstream gust front with maximum magnitude in excess of $0{\cdot}05\,s^{-1}$ (a value which is probably resolution-dependent). Despite the existence of negative vorticity at higher levels, the low-levels

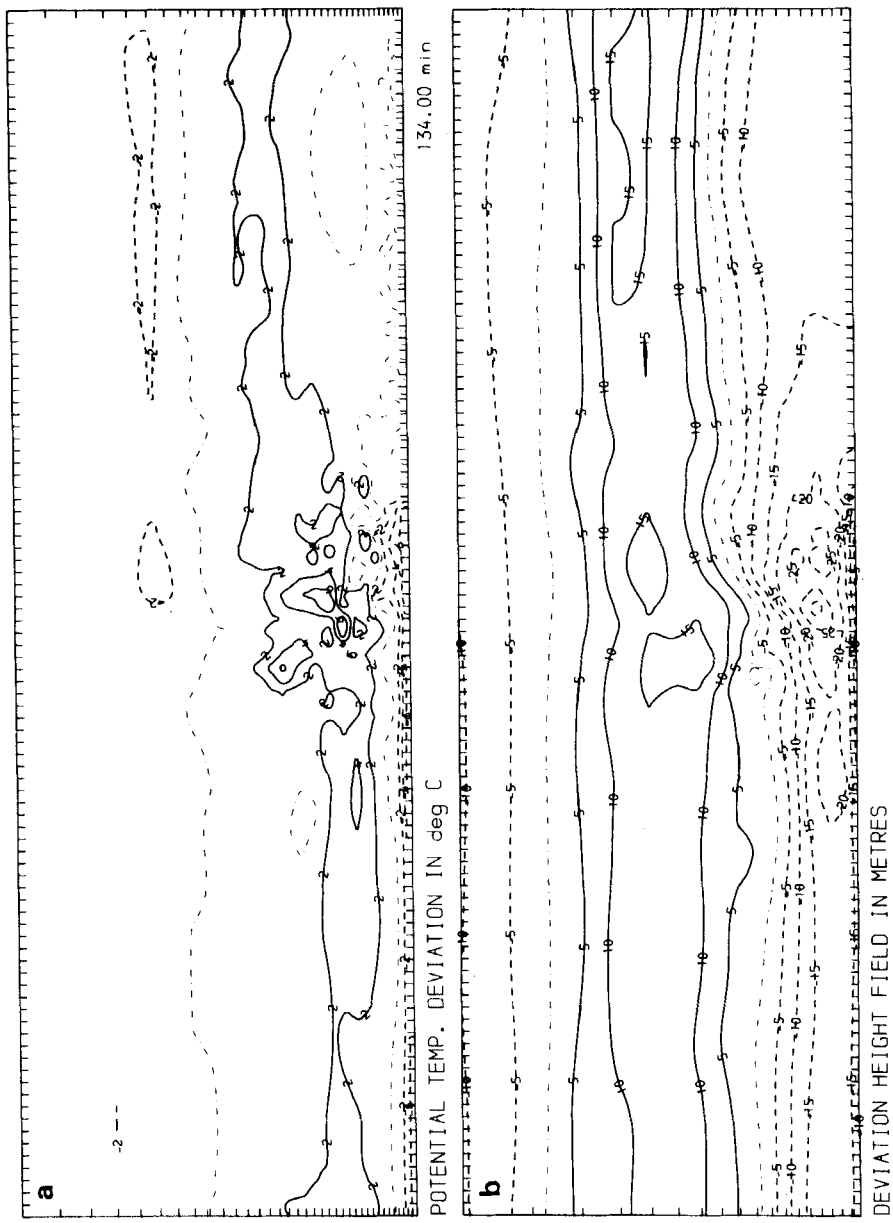

Figure 6. (a) As in Fig. 4 (b) for potential temperature deviation ($\Delta\theta' = 2$K). (b) As in (a) for height deviation ($\Delta h' = 5$ m).

represent the region of maximum values. The positive vorticity of the downdraught circulation is apparent and is about four times that of the low-level inflow. The anvils have opposite sign vorticity to each other. The potential temperature deviation has a structure with strong low-level cooling in the downdraught and a cold dome apparent at the tropopause. As expected, the updraught has large θ' excesses of over 5 °C with warm anvils on both sides of the storm. There is also warming at middle levels over the surface downdraught outflow due to dynamically induced subsidence as air approaches the storm to feed the downdraught circulation.

In Fig. 6(b) the deviation height field is shown and, due to the predominant warming, the remote flow has a hydrostatic pressure distribution with surface low pressure, compared to the *initial* state. Therefore, to obtain the relative deviation from the remote flow, about

13 m must be added to the values in the storm centre. Deviations from hydrostatic balance are apparent in the storm, with a maximum surface meso-high of about 1·3 mb. A noticeable feature of the fields is the mesoscale pressure difference, ΔP, *across* the storm with the following vertical variation ($\Delta P = P_{\text{right}} - P_{\text{left}}$):

$$\begin{aligned} \Delta P &< 0 \qquad P > 950\,\text{mb} \\ \Delta P &> 0 \qquad 950 > P > 700\,\text{mb} \\ \Delta P &< 0 \qquad 700 > P > 300\,\text{mb} \\ \Delta P &\simeq 0 \qquad 300 > P \end{aligned}$$

Such a pressure difference is important and is characteristic of other types of convection (see Moncrieff 1981).

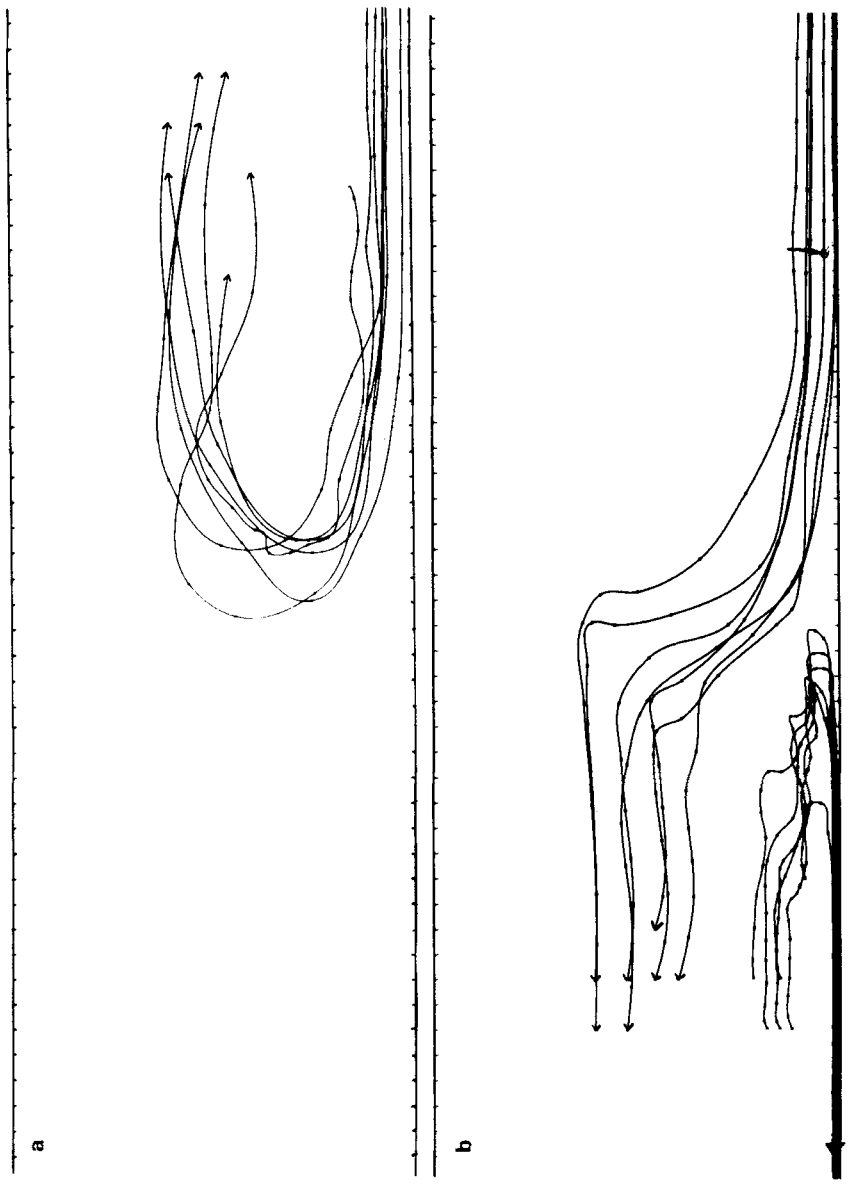

Figure 7. (a) Trajectories in updraught feeding right-side anvil. (b) As in (a) for left-side anvil and downdraught trajectories.

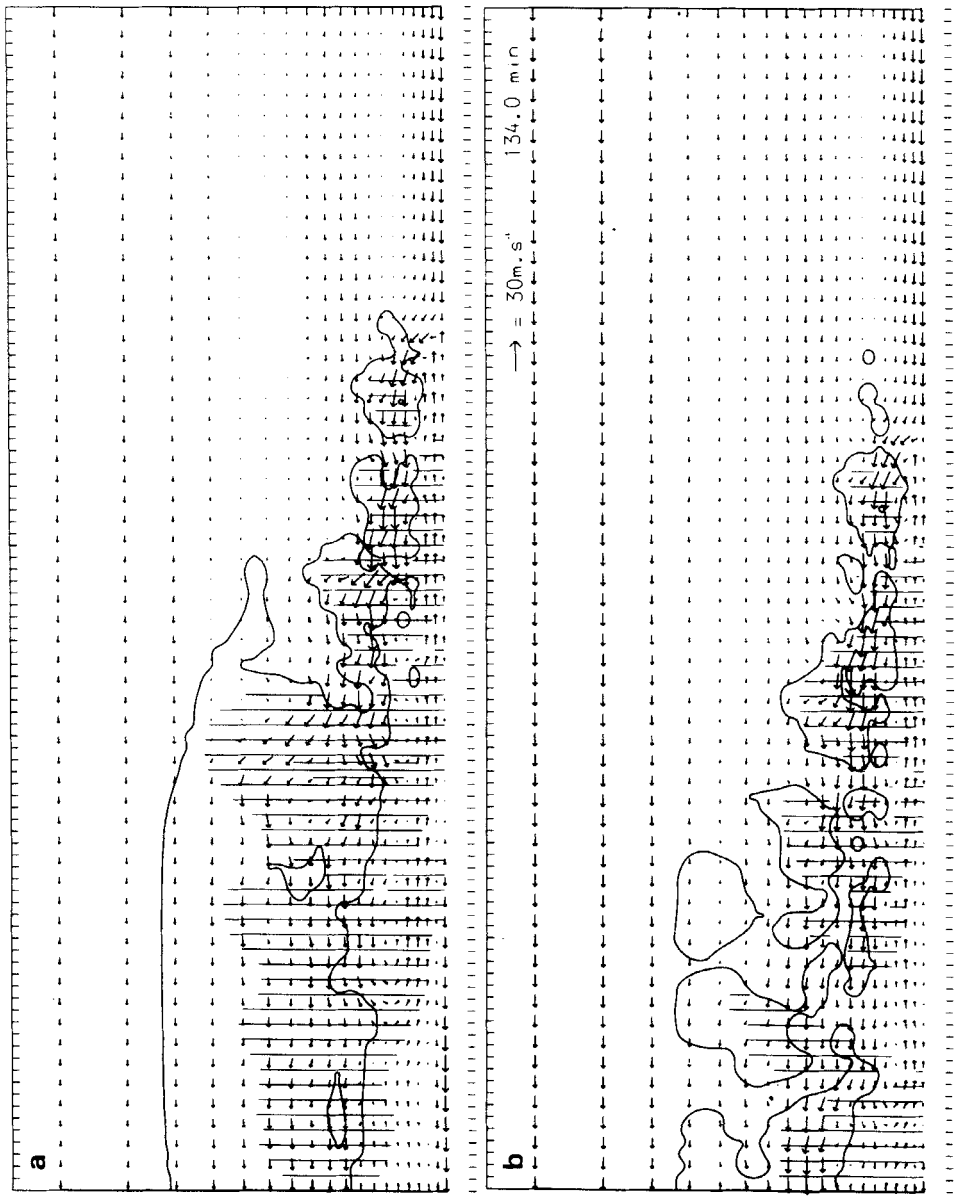

Figure 8. (a) Cloud cross-section at $t = 134$ min for $P(-5)$. (b) As in (a) for $P(-10)$.

The upshear slope of the updraught below about 500 mb is evident. At 64 min the anvil is much more pronounced to the right of the storm, although clearly some cloud is extending to the left. By 134 min the anvil appears to be nearly symmetrical, indicating that the updraught splits into two parts at upper levels. This updraught structure is also shown by the representative trajectories of Fig. 7(a) and (b) and the low-level inflow evidently feeds two updraught flows which produce upper-level outflow to the left and to the right of the storm. Fig. 7(b) shows several trajectories typical of the downdraught circulation. The intersection of trajectories in two-dimensions indicates a degree of unsteadiness.

It is interesting to compare the structure of the storms $P(0)$, $P(-5)$, and $P(-10)$. Cross sections for $P(-5)$ and $P(-10)$ are shown in Fig. 8(a) and 8(b) respectively, at $t = 134$ min. It is apparent that the anvil to the right has been eliminated by the upper level flow and that storm $P(-10)$ has a shallow cellular structure. Also the motion of the

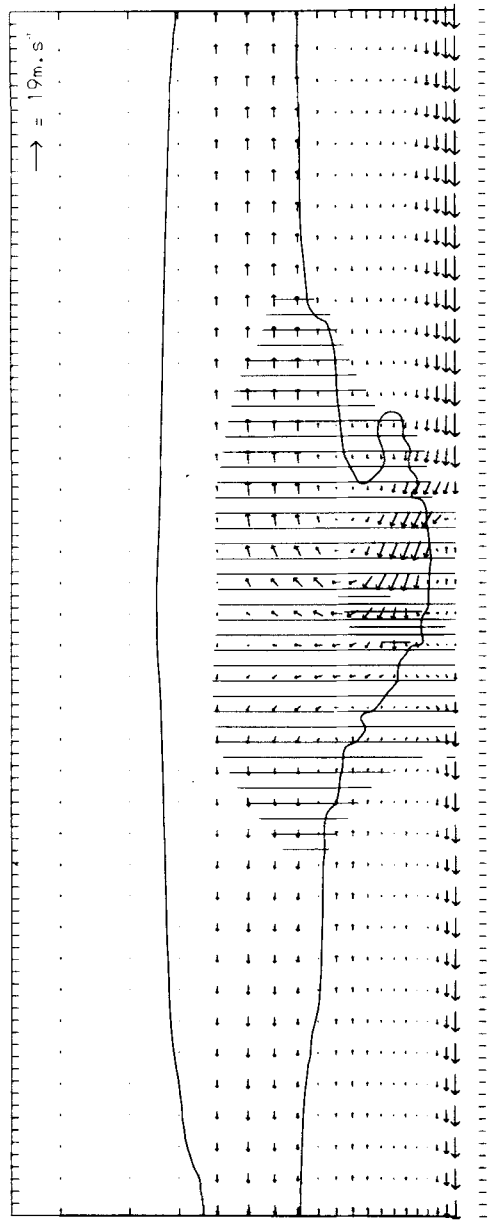

Figure 9. Storm structure of 90–170 min average fields.

upstream gust front, the lighter widespread rainfall, and the increased slope of the updraught, are evident.

(*b*) *Time-averaged structure*

The steadiness of this storm, evident for example in Fig. 3, suggests that computing a time average of the fields will emphasize the essential storm structure, particularly in (differentiated) variables such as vorticity. Figures 9, 10, 11 show the results from an average over the period 90–170 min. The streamfunction of Fig. 10(a) is of particular interest. The dual updraught structure is apparent with the left side anvil being fed by inflow air from the lowest levels. In contrast, the right-hand anvil draws air from above these levels. Perhaps the most crucial difference between these flows is that the right side circulation

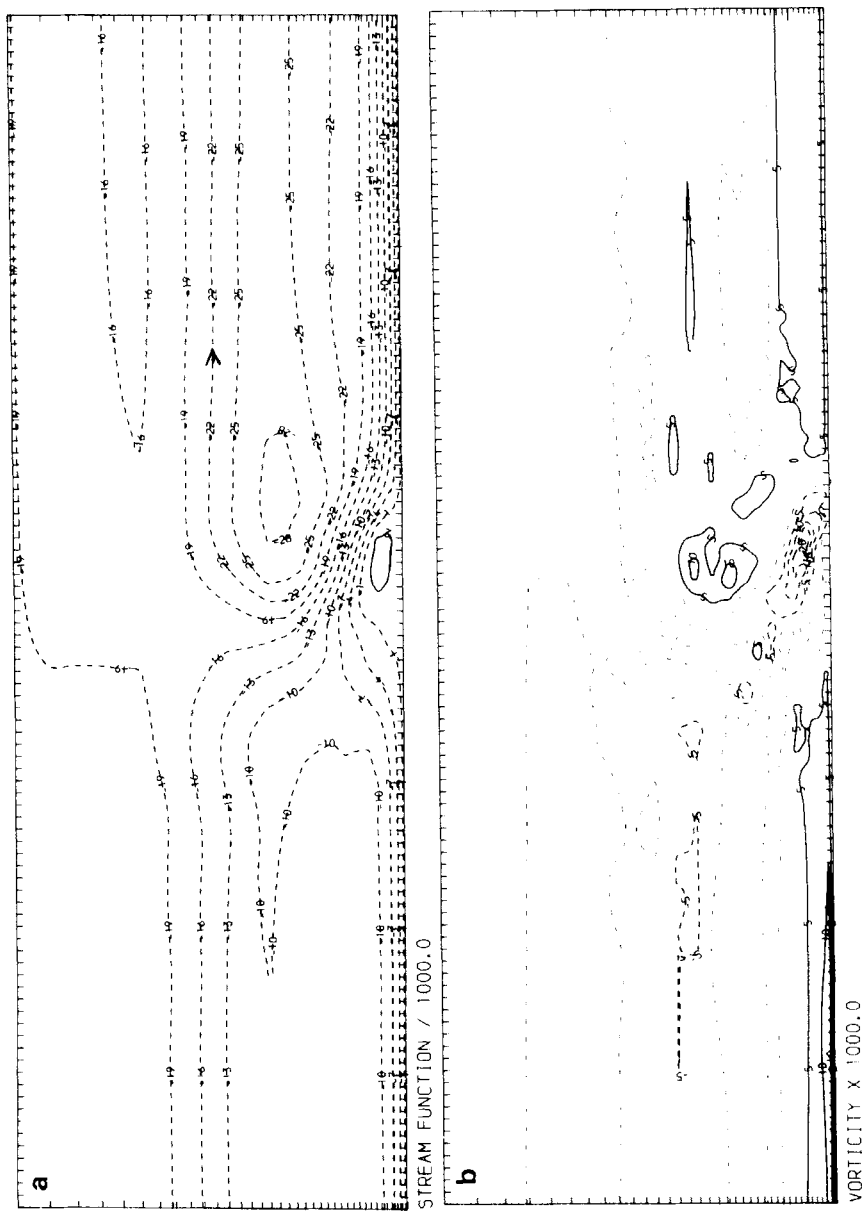

Figure 10. (a) As in Fig. 9 for streamfunction. (b) As in (a) for vorticity.

involves overturning whereas the left side does not, and for this reason the two updraughts can be labelled overturning and jump-type respectively. Inflow air adjacent to the surface does not enter the updraught but ascends over the upstream gust front and descends behind it into the down-draught surface outflow. This part of the flow will be called the boundary layer because it represents air which suffers relatively small displacements from the surface. The upstream density current appears in Fig. 10(a) as a closed cell or rotor beneath the boundary layer. Trajectories show recirculating air in the rotor (producing overlapping lines unsuitable for reproduction). The main downdraught circulation behind the storm is also evident in the streamfunction.

The average vorticity field of Fig. 10(b) has the basic structure described previously, but much of the fine detail has disappeared in the averaging process. Further reference will be made to the vorticity in the next section.

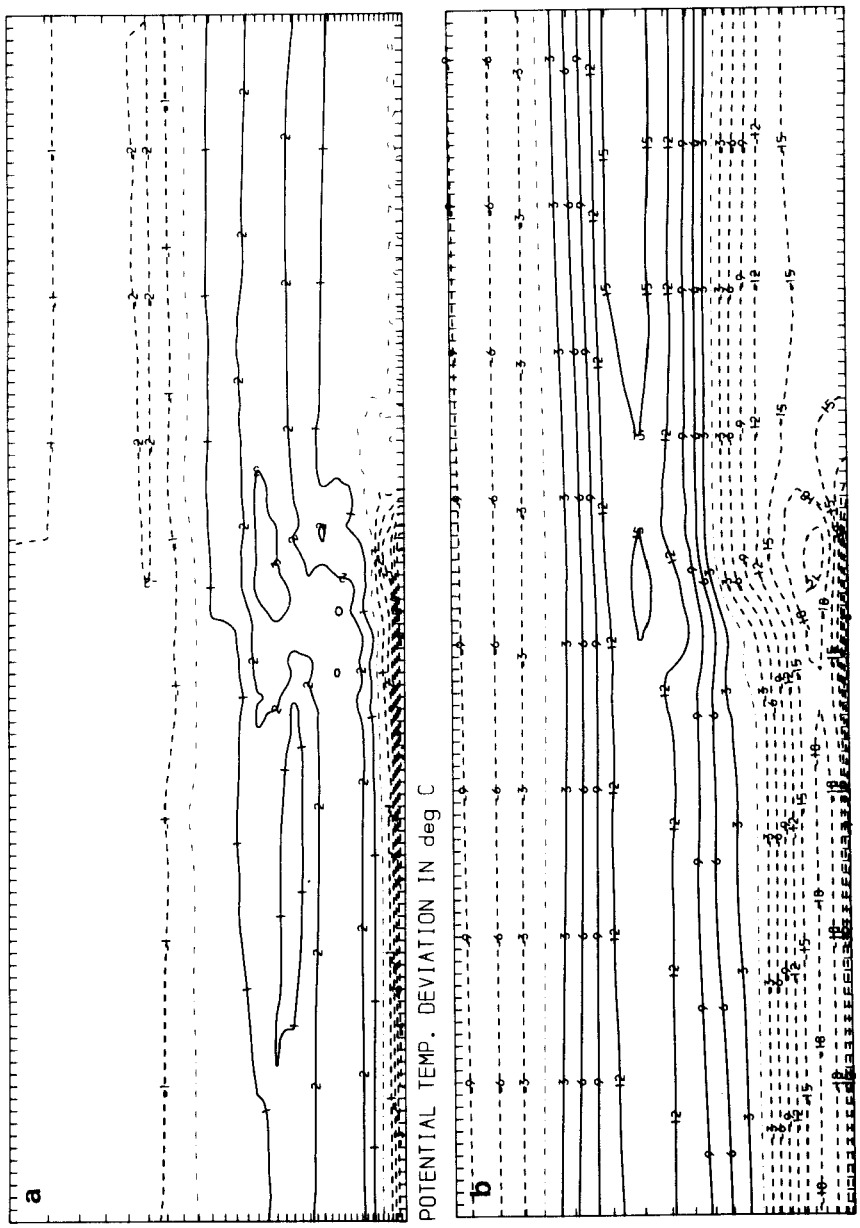

Figure 11. (a) As in Fig. 9 for potential temperature deviation ($\Delta\theta' = 1$ K). (b) As in (a) for height deviation ($\Delta h' = 3$ m).

4. Asymptotic solutions describing an idealized model

The steady state of storm $P(0)$ can be examined using conservation principles for two-dimensional motion. The equations will be applied to an idealized model of the storm, shown in Fig. 12, this being the simplest structure having the essential characteristics of the *remote* flow, which can be analysed theoretically. Complications involving the *internal* structure of the simulated storm, such as the boundary layer and the rotor will be considered in the next section.

(*a*) *Conservation principles*

The equations of motion for steady, inviscid, two-dimensional, incompressible flow

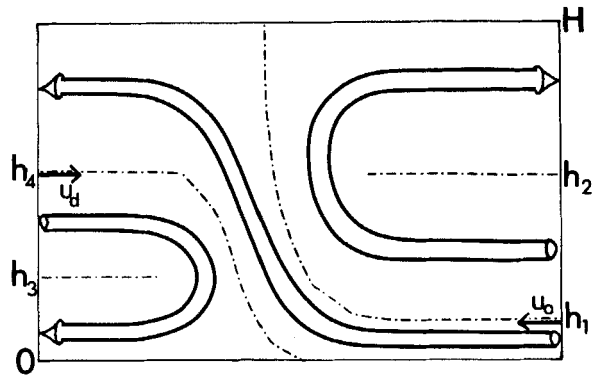

Figure 12. Idealized model with reference heights labelled.

neglecting the Coriolis force, can be manipulated to give several conserved quantities. Assuming an entropy source/sink of the form $w\gamma$ (where γ is a constant parcel lapse rate) and a constant static stability (B) the conserved quantities can be written as

$$\frac{D}{Dt}\left\{\eta + \frac{g(\gamma - B)(z - z_0)}{u_0(z)}\right\} = 0 \quad . \quad . \quad . \quad (1)$$

$$\frac{D}{Dt}\left\{\delta\phi_p - (\gamma - B)(z - z_0)\right\} = 0 \quad . \quad . \quad (2)$$

$$\frac{D}{Dt}\left\{\tfrac{1}{2}\mathbf{v}^2 + \frac{\delta p}{\rho} - \int_{z_0}^{z} g\,\delta\phi_p\,dz\right\} = 0 \quad . \quad . \quad (3)$$

where $\eta = \dfrac{\partial u}{\partial z} - \dfrac{\partial w}{\partial x}$ is the vorticity

$\delta\phi_p = \phi_p - \phi_0$ is the difference between the log potential temperature of a parcel and to the environment

δp is the deviation of pressure from the hydrostatic basic state

$z_0(\psi)$ is a reference (inflow) level of an arbitrary streamline ψ

$u_0(z)$ is the relative inflow speed

Equations (1), (2) and (3) are the vorticity, thermodynamic and energy equations respectively and the quantities in curly brackets are constant (equal to the inflow value) along streamlines in steady motion.

Two further equations will be used in the discussion – a displacement equation and the momentum budget. Equations (2) and (3) and the continuity equation can be combined to give the displacement equation relating the inflow and outflow heights of streamlines applicable at large distances from the storm interior, $x \to \pm\infty$ (see Moncrieff, 1981):

$$\left(\frac{dz_0}{dz_1}\right)^2 = 1 - \frac{\Delta p}{\frac{1}{2}u_0^2} + \frac{g(\gamma - B)}{\frac{1}{2}u_0^2}\left\{\frac{(z_1 - z_0)^2}{2} - \int_{z_*}^{z_1}(z_1 - z_0)\,dz_1\right\} \quad . \quad (4)$$

where z_1 (z_0 is the outflow height of the streamline which entered the system at height z_0, Δp is the pressure deviation at outflow reference level $z_1 = z_*$, and

$\dfrac{dz_0}{dz_1} = \pm\dfrac{u_1}{u_0}$ ratio of outflow to inflow (horizontal) speed.

The steady-state horizontal momentum equation can be written in flux form as:

$$\nabla.(uv) = -\frac{\partial}{\partial x}\left(\frac{\delta p}{\rho}\right)$$

By integrating over a volume V, defined by planes $x = -\infty$, $x = +\infty$, $z = 0$ and $z = H$ and by using the divergence theorem, the momentum budget is obtained:

$$\int_0^H \left\{\left(u^2 + \frac{\delta p}{\rho}\right)_{+\infty} - \left(u^2 + \frac{\delta p}{\rho}\right)_{-\infty}\right\} dz = 0 \qquad . \qquad . \qquad (5)$$

where quantities in the round brackets refer to the asymptotic flow and pressure deviation at large distances from the system, and u may refer to either inflow or outflow. Unlike the displacement equation, which applies to individual streamlines, Eq. (5) is a bulk constraint, and therefore has to be applied to the whole convective system.

(*b*) *Component flows in the idealized model*

The structure of the component flows will now be considered separately using Eqs. (1), (2), (3) and (4) and in subsection (c) the momentum budget (Eq. (5)) will be used as a constraint on the parameters which arise for these components. The reference heights used in the following analysis are shown in Fig. 12.

(*i*) *Overturning updraught*

The structure of this updraught is identical to that of the updraught in the steering-level model, as described in Moncrieff (1981). The inflow to this region can be written as:

$$u_0(z_0) = A_0(h_2 - z_0), \qquad h_1 \leqslant z_0 \leqslant h_2$$

where A_0 is the constant inflow shear.
The solution to the displacement equation can be shown to be:

$$z_0 = h_2 - \beta_0(z_1 - h_2)$$

where

$$\beta_0(\beta_0 - 1) = R_0 = g(\gamma - B)_0/A_0^2$$

The outflow speed $u_1(z_1)$, is obtained from the displacements by using mass continuity ($u_1 = -u_0\, dz_0/dz_1$); the outflow log-potential temperature deviation is simply the displacement multiplied by the lapse-rate difference; and the corresponding pressure deviation is obtained by using the condition that the remote flow is hydrostatic:

$$u_1(z_1) = \beta_0^2 A_0(h_2 - z_1) \qquad h_2 \leqslant z_1 \leqslant H$$

$$\delta\phi_1(z_1) = (\gamma - B)_0(1 + \beta_0)(z_1 - h_2) \qquad ,,$$

$$\frac{\delta p}{\rho}(z_1) = g(\gamma - B)_0(1 + \beta_0)\frac{(z_1 - h_2)^2}{2} \qquad ,,$$

The height h_2 can be shown to be

$$h_2 = \frac{h_1 + \beta_0 H}{(1 + \beta_0)} \qquad . \qquad . \qquad . \qquad (6)$$

The vorticity equation indicates that the vorticity, which is positive on inflow (by definition), becomes larger in this type of updraught due to release of latent heat, consistent with the result $\beta_0 > 1$ derived from the displacement equation.

(*ii*) *Jump updraught*

The structure of this updraught is distinct from the previous one as the air does not overturn. Nevertheless, potential energy can be released by the vertical displacement of parcels. The analysis of the jump updraught is made much simpler by the assumptions of

constant inflow speed, $u_0 = U_0$, and neglect of mixing across the internal boundaries of the region. The value of U_0 is chosen to be a representative value of the sheared inflow profile, i.e.:

$$U_0 = A_0(h_2 - h_1/2)$$

The solution of the displacement equation is:

$$z_0 = z_1 - \varepsilon FH \sinh\left(\frac{z_1 - h_4}{FH}\right) - h_4 \cosh\left(\frac{z_1 - h_4}{FH}\right) \quad . \quad . \quad (7)$$

where $F = |U_0|/\sqrt{g(\gamma - B)H}$ (Froude number)

$$\varepsilon = 1 - \{1 - E + (h_4/FH)^2\}^{1/2}$$

$$E = \Delta p(z_1 = h_4)/\tfrac{1}{2}U^2$$

Application of boundary conditions $z_1(z_0 = 0) = h_4$ and $z_1(z_0 = h_1) = H$ shows that the heights h_1 and h_4 are related to the Froude number and the pressure change (through ε) by

$$\frac{h_1}{H} = 1 - \varepsilon F \sinh\left(\frac{H - h_4}{FH}\right) - \frac{h_4}{H} \cosh\left(\frac{H - h_4}{FH}\right) \quad . \quad . \quad (8)$$

Equation (8) is a transcendental equation for h_4/H as a function of F, E, and h_1/H, and a numerical solution is necessary. An example in Fig. 13 shows the typical variation of h_4/H with the other parameters. It is clear that for $h_1 \leqslant H - h_4$, which is observed in the simulation, a value of $E > 0$ is required and that there is an approximately reciprocal dependence of F upon E for fixed h_1. The following relationship between R_0 and F gives information about a representative value of F:

$$R_0 = \left(\frac{h_2 - h_1}{FH}\right)^2 \quad . \quad . \quad . \quad (9)$$

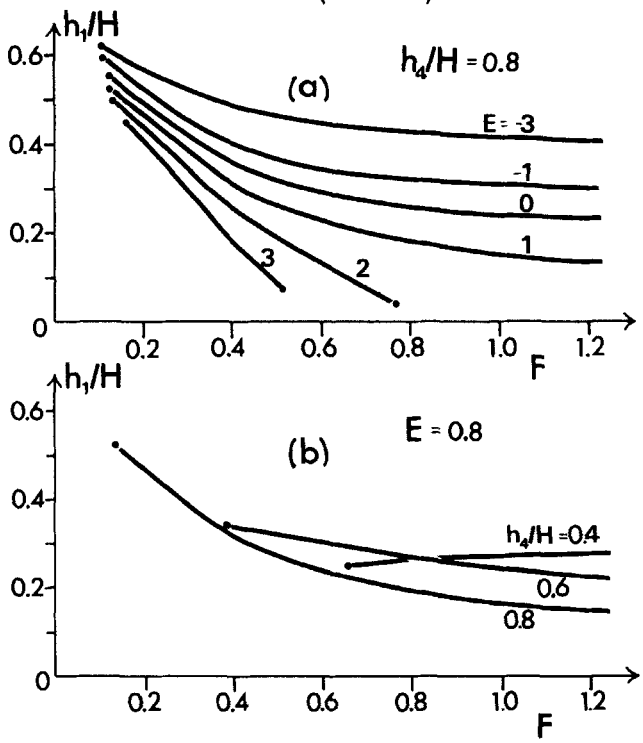

Figure 13. (a) Variation of h_1/H with F for several values of E. (b) Variation of h_1/H with F for several values of h_4/H.

Typical values estimated from the simulations are $R_0 \simeq 0{\cdot}2$ and $(h_2 - h_1)/H \simeq 0{\cdot}4$, giving a value of $F \simeq 0{\cdot}9$, and a value of $E \simeq 1$. The consequent prediction of high pressure deviation on the left of the storm is in accord with the simulation (see Fig. 6(b)).

It is also instructive to examine the vorticity equation with constant u_0 for the jump updraught. As for the overturning updraught, the vorticity increases as the air warms on ascent and the outflow profile has speed decreasing with height, which is in sharp contrast with that of the overturning updraught. The simulation has *negative* vorticity in this region, and so clearly some of the assumptions about this flow are invalid. These problems will be considered in the section on the dynamics of the interior flow.

(iii) *Downdraught*

The downdraught circulation is very similar to that described by the flow labelled *DSC* in TMM and for completeness, it is worth reiterating the results in the present context. The inflow to the downdraught is given by

$$u_0(z_0) = A_d(z_0 - h_3), \qquad h_3 \leqslant z_0 \leqslant h_4$$

where A_d is the constant inflow shear.
The solution to the displacement equation is:

$$z_0 = h_3 + \beta_d(h_3 - z_1)$$

where

$$\beta_d(\beta_d - 1) = R_d = g(\gamma - B)_d/A_d^2$$

In an analogous way to the overturning updraught, the outflow log-potential temperature and pressure deviation profiles are given by the expressions:

$$u_1(z_1) = \beta_d^2 A_d(z_1 - h_3) \qquad 0 \leqslant z_1 \leqslant h_3$$

$$\delta\phi_1(z_1) = (\gamma - B)_d(1 + \beta_d)(z_1 - h_3) \qquad 0 \leqslant z_1 \leqslant h_3$$

$$\delta p/\rho(z_1) = \Delta p/\rho + g(\gamma - \beta)_d(1 + \beta_d)(z_1 - h_3)^2/2 \qquad 0 \leqslant z_1 \leqslant h_3$$

The level of downdraught stagnation, h_3, is given by

$$h_3 = \frac{h_4}{(1 + \beta_d)} \qquad . \qquad . \qquad . \qquad . \qquad (10)$$

As for the overturning updraught, the vorticity equation indicates that the positive inflow vorticity is increased in the downdraught circulation.

(c) *The combined component flows: an idealized model*

The three individual flows can be amalgamated into the idealized model shown in Fig. 12 provided the solutions satisfy the momentum budget of Eq. (5), which constrains the asymptotic solutions. After considerable algebra, the momentum budget equation can be expressed in the following form:

$$\frac{h_4}{H}\left[E + 2\varepsilon\sinh^2\left\{\left(1 - \frac{h_4}{H}\right)\Big/F\right\}\right] + \frac{F}{2}\left\{\varepsilon^2 + (h_4/FH)^2\right\}\sinh\left\{2\left(1 - \frac{h_4}{H}\right)\Big/F\right\} -$$

$$- \left(1 - \frac{h_1}{H}\right)\left(\frac{2\beta_0^3 + 3\beta_0^2 - 1}{3\beta_0(1 + \beta_0)}\right) + \frac{h_4}{H}\left(\frac{U_d}{U_0}\right)^2\left(\frac{2\beta_d^3 + 3\beta_d^2 - 1}{3\beta_d(1 + \beta_d)}\right) = 0$$

This equation is most easily described by rewriting as:

$$\left|\frac{U_d}{U_0}\right| = G\left(\frac{h_4}{H}, F, \beta_0, \beta_d, E, \frac{h_1}{H}\right) \qquad . \qquad . \qquad . \qquad (11)$$

where U_d is the downdraught inflow speed at $z_0 = h_4$.

The asymptotic steady states described in Fig. 13, are solutions to the displacement equation and the momentum budget. The non-dimensional numbers which characterize the

solutions are the set $\left\{\frac{h_1}{H}, \frac{h_2}{H}, \frac{h_3}{H}, \frac{h_4}{H}, F, R_0, R_d, E, U_d/U_0\right\}$. The steady-state model is the solution to an eigenvalue problem in which the eigenvalues, and non-dimensional numbers, are related via Eqs. (6), (8), (9), (10), and (11); there are, therefore, five equations in nine unknowns. However, it is possible to separate the set into two subsets, one containing parameters characterizing the ambient atmosphere $\{h_2/H, R_0, F\}$ and the other characterizing the storm itself $\{h_1/H, h_3/H, h_4/H, R_d, U_d/U_0, E\}$. Such a distinction is somewhat arbitrary but it is suggested by the numerical simulation which, as an initial-value problem, uses certain input variables from the large-scale flow. Thus the problem is reduced to having six unknowns and five equations. As some of the equations are transcendental, this problem may or may not be well posed. Further insight into the eigenvalue problem can be obtained by rewriting Eqs. (9), (6), (8), (10) and (11) in the following way, where a tilda indicates that the parameter belongs to the set characterizing the ambient atmosphere and β_0 and β_d replace, trivially, R_0 and R_d:

$$\tilde{F} = \left(1 - \frac{\tilde{h}_2}{H}\right)(\tilde{\beta}_0/(\tilde{\beta}_0 - 1))^{1/2} \quad . \quad . \quad . \quad (9)'$$

$$\frac{h_1}{H} = -\tilde{\beta}_0\left(1 - \frac{\tilde{h}_2}{H}\right) + \frac{\tilde{h}_2}{H} \quad . \quad . \quad . \quad (6)'$$

$$E = 1 + \left(\frac{h_4}{\tilde{F}H}\right)^2 - \left[1 + \frac{\frac{\tilde{h}_2}{H} - \tilde{\beta}_0\left(1 - \frac{\tilde{h}_2}{H}\right) + \frac{h_4}{H}\cosh\left\{\frac{1 - h_4/H}{\tilde{F}}\right\} - 1}{\tilde{F}\sinh\left\{\left(1 - \frac{h_4}{H}\middle/\tilde{F}\right)\right\}}\right]^2 \quad (8)'$$

$$\frac{h_3}{H} = \frac{h_4}{H}\frac{1}{(1 + \beta_d)} \quad . \quad . \quad . \quad (10)'$$

$$\left|\frac{U_d}{U_0}\right| = G'\left(\frac{h_4}{H}, \tilde{\beta}_0, \frac{\tilde{h}_2}{H}\right)\left\{\frac{3\beta_d(1 + \beta_d)}{2\beta^3{}_d + 3\beta^2{}_d - 1}\right\}^{1/2} \quad . \quad . \quad (11)'$$

Equation (9)′ demonstrates that there are only two independent parameters $(\tilde{h}_2/H, \tilde{\beta}_0)$ in the set describing the ambient atmosphere and $\tilde{F}$ is simply related to them. Equation (6)′ gives the jump updraught inflow depth in terms of the ambient atmospheric parameters, whilst Eq. (8)′ specifies E as a function of h_4/H and $(\tilde{\beta}_0, \tilde{h}_2/H)$. Equation (10)′ does not involve ambient parameters and Eq. (11)′ gives the velocity ratio $|U_d/U_0|$ as a function of h_4/H and β_d and $(\tilde{\beta}_0, \tilde{h}_2/H)$. It is now relatively easy to see that there are probably several allowed values of $(h_4/H, \beta_d)$ given that $(\tilde{\beta}_0, \tilde{h}_2/H)$ are specified.

The lack of a unique solution is not surprising and is also a feature of tropical squall lines described in Moncrieff and Miller (1976), in which solutions exist for all values of E between 0 and 1. In that paper, a closure hypothesis of maximum convective efficiency was invoked to isolate a solution of particular interest. A different closure technique will be explored in this paper suggested by the internal structure of the simulation. For the interface between the jump updraught and the downdraught to be orientated so as to allow rain to fall from updraught to downdraught, a further constraint on the asymptotic solutions exists. Consider the total energy, as given in Eq. (3), on streamlines on either side of this interface:

$$\tfrac{1}{2}\mathbf{V}_u^2 + \left(\frac{\delta p}{\rho}\right)_u - \tfrac{1}{2}g(\gamma - B)z^2 = \tfrac{1}{2}U_0^2$$

$$\tfrac{1}{2}\mathbf{V}_d^2 + \left(\frac{\delta p}{\rho}\right)_d - \tfrac{1}{2}g(\gamma - B)(z - h_4)^2 = \tfrac{1}{2}U_d^2 + \tfrac{1}{2}U_0^2 E$$

The dynamical boundary condition along the interface is that $\delta p/\rho$ be continuous there,

which gives the equation

$$\Delta(\mathbf{V}^2) = \mathbf{V}_u^2 - \mathbf{V}_d^2 = U_0^2(1-E) - U_d^2 + g(\gamma - B)z^2 - g(\gamma - B)(z - h_4)^2$$

For an upshear slope near the surface, $z \simeq 0$, we require $\Delta(\mathbf{V}^2) > 0$ giving the inequality

$$\left|\frac{U_d}{U_0}\right| < \left\{\frac{(1-E)\beta_d}{\beta_d^3 + \beta_d^2 - 1}\right\}^{\frac{1}{2}} \quad . \quad . \quad . \quad (12)$$

Implicit in this relation is that $E < 1$ and $\left|\frac{U_d}{U_0}\right| < 1$ which are powerful constraints on the eigenvalue problem. Equation (12) constrains the solutions of Eqs. (8)′ and (11)′, giving a rather smaller set of allowed values of $(\beta_d, h_4/H)$ than would otherwise have been obtained. An example of the full solution is shown in Fig. 14. Choosing $\tilde{h}_2/H$ and $\tilde{\beta}_0$ simply predicts $\tilde{F}$ and h_1/H, and the graph shows h_4/H as a function of β_d and E. The allowed values of h_4/H are indicated by the shaded region, the limits for which are given by $U_d/U_0 = 0$ from Eq. (11)′ and the value of $|U_d/U_0|$ required to give an upshear slope from Eq. (12).

Clearly the momentum budget can be satisfied for $U_d = 0$ (no downdraught) and whilst the downdraught is crucial for the internal dynamics as a mechanism for lifting the boundary layer air into the updraught, it is responsible for a relatively minor part of the momentum flux. If, for example, $\beta_d = 1{\cdot}5$, then the slope constraint requires $|U_d/U_0| \lesssim 0{\cdot}36$, which indicates that the downdraught inflow is small compared to that of the updraught. This result agrees well with the simulation.

In summary, the idealized model has enabled the asymptotic flows to be analysed and has indicated the region of parameter space for which the storm is steady. In particular, the solutions are characterized by $E \lesssim 1$, $|U_d/U_0| < 1$, $H - h_4 \geqslant h_1$, and $F \lesssim 1$.

5. Dynamics of the interior flow

Although the idealized model of the asymptotic flow has the advantage of demonstrating analytical solutions, it does not include some distinctive features of the simulated storm $P(0)$. In particular, the shear of the outflow from the idealized jump updraught is positive, whereas the simulation indicated negative vorticity in this region. In this section, details of the interior flow will be examined in an attempt to resolve this discrepancy and it

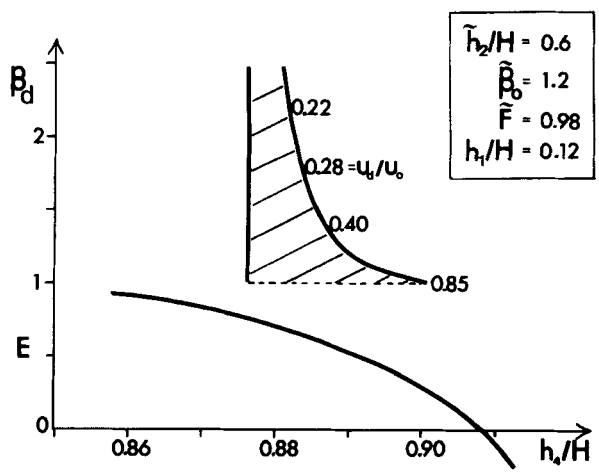

Figure 14. Shaded region of allowed values of h_4/H as a function of βj with limit values of U_d/U_0, from the slope constraint, indicated. Also shown is the variation of E. Input values of h_2/H and $\tilde{\beta}_0$ (and hence $\tilde{F}$ and h_1/H) given in box.

will be postulated that the interface between jump updraught and downdraught is dynamically unstable, leading to the more complex structure of the simulated storm. To aid this discussion, a conceptual model deduced from the simulation is shown in Fig. 15, in which forthcoming nomenclature is defined.

The simulated storm $P(0)$ exhibits two characteristic flows not considered in the idealized model – the boundary layer and the rotor.

(*a*) *Boundary layer*

This flow has been found in many simulations, both of two- and three-dimensional convection, described by this and other numerical models. It exists because the air nearest the surface cannot readily be lifted into the main updraught core. Potentially buoyant air is lifted over the rotor, or upstream-propagating density current, and begins to release latent heat. However, because of its large horizontal momentum, it enters the region of strong cooling under the rain area and eventually descends to the layer near the surface. As evaporative cooling is greater than condensation heating along the trajectory, parcels arrive at the surface with large negative $\delta\theta$. In the equations described previously, this can be represented by a larger γ for $w < 0$. The positive vorticity increases as the air rises, but there is large generation of negative vorticity as the air enters the cooling region. When the parcel leaves the cooling region, positive vorticity is generated again sufficiently to establish positive vorticity in the outflow from this layer.

(*b*) *Rotor*

The rotor, which represents the head of the upstream propagating density current, is similar to the cellular convection model described by Moncrieff (1981). In this case, the motion is driven by evaporative cooling on the left-hand side of the rotor, and so is the downdraught counterpart of the cellular model, which is driven by buoyant upward convection. For the air to recirculate and be in a steady state, there is as much warming as the air rises on the right of the rotor as there is cooling in the downdraught region. However, with no condensation, the rising air is negatively buoyant and so can warm only by mixing across the interface with the boundary layer. The air in the boundary layer is about 6 °C warmer than the adjacent air in the rotor, and so represents an available source of heat. As there are strong gradients of both potential temperature and velocity, the sub grid-scale parametrization ensures downgradient mixing. (There is, however, no physical reason for mixing as warm air overlies colder air, unless sufficiently large gradients in velocity exist at the interface. The simulation produces velocities in the rotor less than those in the boundary layer, and consequently the interface has a large vorticity minimum. Hence the parametrization is acting in a consistent way.)

(*c*) *Interfacial properties*

It is clear from the discussion of the structure of the individual flows in the previous

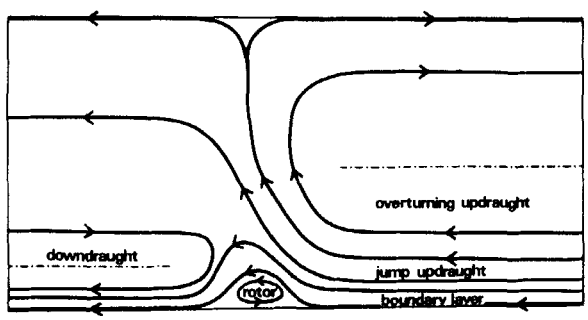

Figure 15. Conceptual model, derived from Fig. 9, with individual flows labelled.

subsection that interactions at the interfaces between the distinct types of flow are dynamically important. The two main regions of interaction are between the rotor and the boundary layer and between the jump updraught and the boundary layer.

For the rotor to exist in a steady state there must be mixing at the interface with the boundary layer, which introduces warming of rotor parcels and cooling of boundary layer air. This also explains why the boundary layer air is unsuitable for inclusion in the jump updraught and, indeed, why the surface outflow from the storm is not potentially unstable; a situation which would occur if parcels in the boundary layer conserved equivalent potential temperature (c.f. lower θ_e of downdraught air). This discussion is inevitably qualitative as the boundary layer, although crucial, is rather shallow, being on inflow about the vertical grid-length of the numerical model. It is easy to show that the velocity difference between rotor and the boundary layer implies an upshear slope to the interface, using an argument similar to that in the previous section.

It is apparent from the streamline pattern of the simulated storm that there is a layer of inflow which takes part in neither the jump updraught nor the boundary layer flow. Individual trajectories show that parcels entering this region undergo turbulent mixing. The details of the dynamics are therefore difficult to describe, but the effect on the jump updraught appears to be very important. The jump updraught produces an anvil in the simulation which has predominantly negative vorticity, whereas, as argued in the previous section, Eq. (1) suggests that it should have positive vorticity. There are two processes which can add negative vorticity into this airstream – cooling in middle levels due to rainwater and cloud water evaporation, and mixing at the lower interface of the layer. The first obviously occurs and, because of the slope of the updraught, has a greater effect in the jump than the overturning updraught but this is difficult to quantify. As argued for the rotor/boundary layer interface, there is probably negative vorticity present at the lower interface of the jump updraught due to the reduction in kinetic energy of the turbulent air below.

(*d*) *Relationship to previous conceptual models*

The conceptual model of storm $P(0)$ may be compared with that studied previously by Moncrieff (1978), in which assumptions of constant shear and deep downdraughts were made, and it was shown that steady convection could not exist because the downdraught sloped *downshear* over the updraught and hence could not be maintained by cooling due to raindrop evaporation. The upper box in Fig. 16(a) is a schema of the steady state taken from Moncrieff (1978) and, as described by Eq. (17) of that paper, the interface between updraught and downdraught is a downshear orientated vortex sheet with a velocity-square difference given by:

$$\Delta(\mathbf{V}^2) = 2HA^2R(z - H/2)$$

Moreoever, this vortex sheet is dynamically unstable and the solution to the initial-value problem shows that at least for sufficiently large values of R ($R \sim 1$), closed cells are produced between updraught and downdraught (see Fig. 16(a)). At the ground (and the 'tropopause') a rotor may exist representing an upstream-propagating density current.

Analogous arguments can be applied to the idealized model of the storm $P(0)$ described in Section 4. This is shown in the upper box of Fig. 16(b). Again a vortex sheet exists, as indicated by the dashed line in this figure, which is likely to break down into eddies as a consequence of instability, with the possibility of a near-surface rotor emerging. The final structure of the conceptual model in Fig. 16(b) is that deduced from the simulation results. As in constant shear, there is no reason, *a priori*, for supposing that the updraught slope will be backward-sloping, but the lack of upper-level mean flow clearly allows this to exist in a steady state in the simulation. Consequently, the inclusion of shallow downdraughts, non-constant shear and a *cross-storm pressure gradient* results in a basically different type of steady convection from that considered in Moncrieff (1978) in that the orientation of the updraught is consistent with an evaporatively driven downdraught.

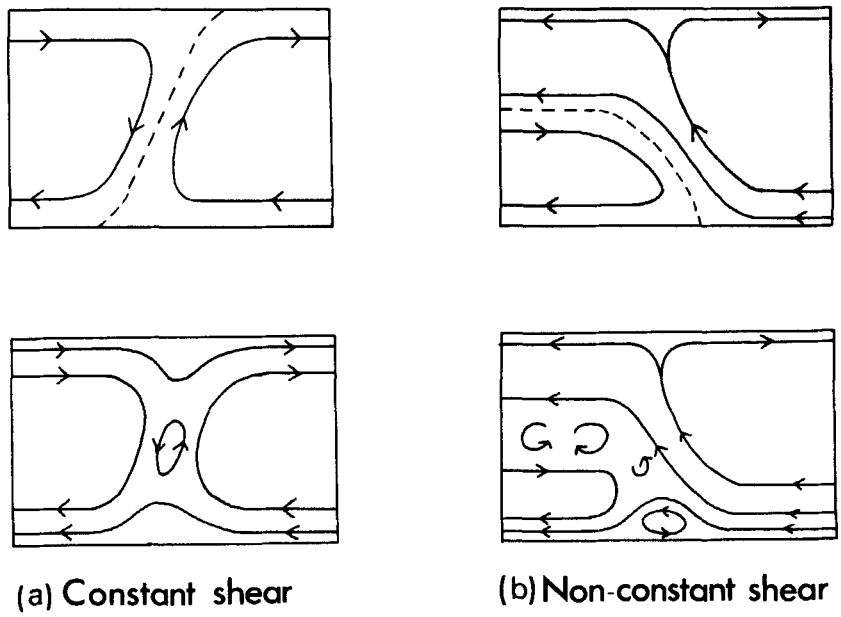

Figure 16. (a) Convection in constant shear with a deep downdraught, schematically showing the steady analytical solution with interfacial vortex sheet (– – –) and the solution to the initial-value problem. (b) As in (a) for non-constant shear and a shallow downdraught.

6. Discussion

The dynamical structure of storm $P(0)$ has been analysed in some detail, using the time-average fields and the conservation principles derived in the steady theory. It is apparent that in two-dimensions, the most efficient and steady storm occurs when there is strong low-level shear and weak mid- and upper-level shear. Furthermore, the storm involves only one cell and so can be classified as a two-dimensional supercell. Although attention has been focused on $P(0)$, storms $P(-5)$, $P(+5)$ require future analysis because of their persistence.

A distinctive downdraught initiation technique has been used to generate the necessary low-level convergence. However, it is believed that this does not affect the steady state. For comparison, the case $P(0)$ was rerun using a more conventional warm bubble initiation, which involved heating a region 2·5 km in length and 50 mb in depth for 3 min to produce a temperature perturbation of 1·8 °C at 925 mb. The resulting convection had an extremely slow growth, but once rain and a downdraught were produced, more vigorous overturning began. There were strong similarities, suggesting that perhaps the steady state may not be too strong a function of initiation mechanism. However, the growth rate, and to some extent the intensity of the storm, is clearly dependent on the initiation.

The downdraught mechanism described in this paper has an interesting parallel with orographic forcing in that the cold dome of air produced at the surface acts like an obstacle to the flow. Assuming a steady state, the interface between the updraught and the downdraught can be imagined to represent an equivalent hillside. It is interesting, in this context, to examine the pre-storm sounding relevant to the big Thompson Canyon storm of 31 July, 1976 (Caracena *et al.* 1979). This devastating stationary storm gave exceptional rainfall over the eastern slopes of the Rockies. There was large low-level shear with rather weak mid- and upper-level flow similar to the $P(0)$ profile. From the available observations it has been suggested that there was little or no downdraught surface outflow on this occasion and that the mountain slope was responsible for keeping the storm stationary. The simulation of $P(0)$ implies that the downdraught gust front acts in a similar way to the mountain, so that although the Big Thompson Storm needed orographic forcing, the structure can also be

produced with no orography in the presence of a downdraught circulation. There are several other examples quoted in Caracena *et al.* (1979) of stationary storms in such wind profiles.

Observations of mid-latitude squall lines described by Newton (1966), Hane (1973) and Ogura and Liou (1980) indicate that storm $P(0)$ has many of the characteristics of such lines. It seems that prefrontal synoptic conditions in central and eastern U.S.A. can lead to the existence of surface convergence, available potential energy, and a wind profile similar to $P(0)$. Many of the properties of the mid-latitude squall line described by Ogura and Liou are reproduced in the simulation $P(0)$ – ambient flow profile, anvils both forward and rear of the line, vigorous low-level downdraught fed from middle levels behind and low levels in front of the line (i.e., downdraught and boundary layer of the conceptual model), and middle level subsidence and warming. Further observations of mid-latitude squall lines should be examined to test these hypotheses. Ogura and Liou attempt to point to similarities with tropical squall lines but a crucial difference is apparent in that the tropical lines move *faster* than the tropospheric winds, thus usually giving inflow at all levels ahead and outflow behind the line. The mid-latitude lines appear to draw middle-level air into the downdraught from behind the line and also probably move with a mid- or upper-steering level. It is possible that these differences are related to an inherently three-dimensional structure of tropical squall lines (see Moncrieff and Miller 1976) distinct from the two-dimensionality of their mid-latitude counterparts.

Acknowledgments

The authors would like to thank Dr J. S. A. Green for many illuminating discussions on this topic, and Mr A. G. Seaton for programming and graphics work. Also, Dr Thorpe would like to acknowledge receipt of N.E.R.C. financial support for this research.

References

Caracena, F., Maddox, R. A., Hoxit, L. R. and Chappell, C. F. 1979 Mesoanalysis of the Big Thompson Storm. *Mon. Wea. Rev.*, **107**, 1–17.

Clark, T. L. 1979 Numerical simulations with a three-dimensional cloud model: lateral boundary experiments and multicellular severe storm simulations. *J. Atmos. Sci.*, **36**, 2191–2215.

Hane, C. 1973 The squall line thunderstorm: Numerical experimentation. *Ibid.*, **30**, 1672–1690.

Klemp, J. B. and Wilhelmson, J. B. 1978 Simulations of right and left moving storms produced through storm splitting. *Ibid.*, **35**, 1097–1110.

Miller, M. J. 1978 The Hampstead Storm: a numerical simulation of a quasi-stationary cumulonimbus system. *Quart. J. R. Met. Soc.*, **104**, 413–427.

Miller, M. J. and Thorpe, A. J. 1981 Radiation conditions for the lateral boundaries of limited-area numerical models. *Ibid.*, **107**, 615–628.

Moncrieff, M. W. 1978 The dynamical structure of two-dimensional steady convection in constant vertical shear. *Ibid.*, **104**, 543–567.

1981 A theory of organized steady convection and its transport properties. *Ibid.*, **107**, 29–50.

Moncrieff, M. W. and Green, J. S. A. 1972 The propagation and transfer properties of steady convective overturning in shear. *Ibid.*, **98**, 336–352.

Moncrieff, M. W. and Miller, M. J. 1976 The dynamics and simulation of tropical cumulonimbus and squall lines. *Ibid.*, **102**, 373–394.

Newton, C. W. 1966 Circulations in large sheared cumulonimbus. *Tellus*, **18**, 699–712.

Ogura, Y. and Liou, M.-T. 1980 The structure of a mid-latitude squall line: a case study. *J. Atmos. Sci.*, **37**, 553–567.

Orville, H. D. 1968 Ambient wind effects on the initiation and development of cumulus cloud over mountains. *Ibid.*, **25**, 385–403.

Schlesinger, R. E. 1973 A numerical model of deep moist convection: Part I. Comparative experiments for variable ambient moisture and wind shear. *Ibid.*, **30**, 835–856.

Takeda, T. 1971 Numerical simulation of a precipitating convective cloud: The formation of a long-lasting cloud. *Ibid.*, **28**, 350–376.

Thorpe, A. J., Miller, M. J. and Moncrieff, M. W. 1980 Dynamical models of two-dimensional downdraughts. *Quart. J. R. Met. Soc.*, **106**, 463–484.

Wilhelmson, R. B. 1974 The life cycle of a thunderstorm in three dimensions. *J. Atmos. Sci.*, **31**, 1692–1751.